Liquid Crystals
Publication details, including instructions for authors and subscription information:
http://www.informaworld.com/smpp/title~content=t713926090

Cubic phase of 4'-*n*-Hexadecyloxy-3'-cyanobiphenyl-4-carboxylic acid (ACBC-16)

Shoichi Kutsumizu[a]; Kazuya Saito[bc]; Shuichi Nojima[d]; Michio Sorai[b]; Yuri G. Galyametdinov[ef]; Irina Galyametdinova[ef]; Rudolf Eidenschink[g]; Wolfgang Haase[e]
[a] Department of Chemistry, Faculty of Engineering, Gifu University, 1-1 Yanagido, Gifu 501-1193, Japan [b] Research Center for Molecular Thermodynamics, Graduate School of Science, Osaka University, Toyonaka, Osaka 560-0043, Japan [c] Department of Chemistry, Graduate School of Pure and Applied Sciences, University of Tsukuba, Tsukuba, Ibaraki 305-8571, Japan [d] Graduate School of Science and Engineering, Tokyo Institute of Technology, 2-12-1 O-okayama, Meguro-ku, Tokyo 152-8552, Japan [e] Institut für Physikalische Chemie, Fachgebiet Kondensierte Materie, Technische Universität Darmstadt, Petersenstrasse 20, D-64287 Darmstadt, Germany [f] Kazan Physical-Technical Institute, Russian Academy of Sciences, Sibirsky Tract 10/7, 420029 Kazan, Russia [g] NEMATEL, Galileo-Galilei Strasse 28, D-55129 Mainz-Hechtsheim, Germany

To cite this Article Kutsumizu, Shoichi , Saito, Kazuya , Nojima, Shuichi , Sorai, Michio , Galyametdinov, Yuri G. , Galyametdinova, Irina , Eidenschink, Rudolf and Haase, Wolfgang(2006) 'Cubic phase of 4'-*n*-Hexadecyloxy-3'-cyanobiphenyl-4-carboxylic acid (ACBC-16)', Liquid Crystals, 33: 1, 75 — 84
To link to this Article: DOI: 10.1080/02678290500445956
URL: http://dx.doi.org/10.1080/02678290500445956

Liquid Crystals, Vol. 33, No. 1, January 2006, 75–84

Cubic phase of 4′-*n*-Hexadecyloxy-3′-cyanobiphenyl-4-carboxylic acid (ACBC-16)

SHOICHI KUTSUMIZU*†, KAZUYA SAITO‡§, SHUICHI NOJIMA¶, MICHIO SORAI‡, YURI G. GALYAMETDINOV††‡‡, IRINA GALYAMETDINOVA††‡‡, RUDOLF EIDENSCHINK§§ and WOLFGANG HAASE††

†Department of Chemistry, Faculty of Engineering, Gifu University, 1-1 Yanagido, Gifu 501-1193, Japan
‡Research Center for Molecular Thermodynamics, Graduate School of Science, Osaka University, Toyonaka, Osaka 560-0043, Japan
§Department of Chemistry, Graduate School of Pure and Applied Sciences, University of Tsukuba, Tsukuba, Ibaraki 305-8571, Japan
¶Graduate School of Science and Engineering, Tokyo Institute of Technology, 2-12-1 O-okayama, Meguro-ku, Tokyo 152-8552, Japan
††Institut für Physikalische Chemie, Fachgebiet Kondensierte Materie, Technische Universität Darmstadt, Petersenstrasse 20, D-64287 Darmstadt, Germany
‡‡Kazan Physical-Technical Institute, Russian Academy of Sciences, Sibirsky Tract 10/7, 420029 Kazan, Russia
§§NEMATEL, Galileo-Galilei Strasse 28, D-55129 Mainz-Hechtsheim, Germany

(*Received 4 April 2005; in final form 31 August 2005; accepted 5 September 2005*)

The cubic phase structure of 4′-*n*-hexadecyloxy-3′-cyanobiphenyl-4-carboxylic acid (ACBC-16) was examined by X-ray diffraction. Unlike the octadecyloxy homologue showing an *Im*3*m*-type cubic phase, the cubic phase of ACBC-16 was of *Ia*3*d* type, both on heating and on cooling, similarly to the corresponding nitro-substituted analogue (ANBC-16). The lattice dimension a at 453 K was $a=11.0$ nm, 2.5% larger than the value for ANBC-16 and rather close to the value of ANBC-17 or -18. It is expected that the appearance of the cubic phase type, as a function of the number of carbon atoms n in the alkoxy chain in the ACBC-*n* series, is essentially the same as in the ANBC-*n* series, but shifted towards shorter n by 1 or 2. In the latter ANBC-*n* series, the cubic phase type is *Ia*3*d* for $15 \leqslant n \leqslant 18$, while an *Im*3*m* type is formed for $19 \leqslant n \leqslant 21$, both on heating and on cooling.

1. Introduction

4′-*n*-Alkoxy-3′-nitrobiphenyl-4-carboxylic acids ($X=NO_2$ in Scheme 1 and designated as ANBC-*n*, where n is the number of carbon atoms in the alkoxy tail) and 4′-*n*-alkoxy-3′-cyanobiphenyl-4-carboxylic acids ($X=CN$ in Scheme 1 and designated as ACBC-*n*) are well known as mesogens exhibiting thermotropic cubic (Cub) phases. Both series of compounds (which include ANBC-*n* with $n=1$–10, 12, 16 and 18 [1], and ACBC-*n* with $n=16$ and 18 [2, 3]) were first synthesized by Gray and his co-workers. The Cub phases of ANBC-*n* were characterized by Sackmann and co-workers [4–6]. Since then, much attention has been paid to the phase behaviour of ANBC-*n* and our knowledge on the Cub phases has been greatly advanced [7–33]. The alkoxy chain length, n, is a key factor in forming Cub phases; the Cub phase appears when $n \geqslant 15$, and its temperature region is monotonously increased with increasing n [10]. The Cub region that had been assumed to consist of a single phase was found to contain two types of Cub phase, one with *Im*3*m* symmetry (and denoted Cub I in this paper) and the other with *Ia*3*d* (Cub II) [18, 21, 22, 26, 27]; the type of the cubic phase depended on n, with *Ia*3*d* for $15 \leqslant n \leqslant 18$, *Im*3*m* for $19 \leqslant n \leqslant 21$, both on heating and on cooling. A complicated feature of the Cub phase region is that the *Ia*3*d* region appears again in the high temperature region of $n=22$ and 26 homologues, and as a result, the *Im*3*m* region intervenes between the two regions of the *Ia*3*d* phase. For $n=22$ and 26, a cubic-to-cubic phase transition was observed at a mid temperature in the Cub region, on heating, but only the *Ia*3*d* type was observed on cooling. Adiabatic calorimetric [15, 17, 25] and high pressure investigations [20, 24, 32, 33] were also carried out

*Corresponding author. Email: kutsu@cc.gifu-u.ac.jp

Liquid Crystals
ISSN 0267-8292 print/ISSN 1366-5855 online © 2006 Taylor & Francis
http://www.tandf.co.uk/journals
DOI: 10.1080/02678290500445956

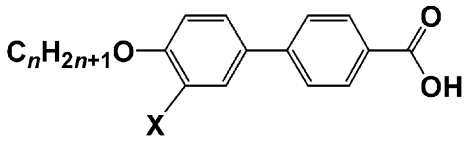

Scheme 1. Chemical structure of ANBC-*n* (X=NO_2) and ACBC-*n* (X=CN).

and valuable insights into the Cub phase formation have been obtained including a quasi-binary system model [23, 30, 31] and information on the stability of the Cub phases as a function of pressure as well as temperature.

Compared with the ANBC-*n* series, publications for the ACBC-*n* series are surprisingly scarce, probably because of the difficulty in synthesis of this series. The phase sequences of the $n=16$ and $n=18$ members are [2, 3]:

ACBC-16[3] :

404 K 439 K 474 K

Cr ⇄ SmC ⇄ Cub ⇄ I_1 ⇄ I_2

417–426 K 473 K

ACBC-18[3] :

404 K 429 K 474 K

Cr ⇄ SmC ⇄ Cub ⇄ I_1 ⇄ I_2

411 K 473 K

Here, the subscripts of the I represent the classification of isotropic liquid states, which will be described later (see §4.2). Except for the X-ray studies mentioned later, there has only been a recent report on the heat capacity for ACBC-16 by Sorai *et al.* [34]. The structure of the Cub phase was first studied by Etherington *et al.* for ACBC-18 and they identified the phase type as being *Pm*3*m* or *Pm*3 [35, 36]. Levelut and Fang [9] and Levelut and Clerc [12] re-examined the structure of the Cub phase of ACBC-18 and showed that it belongs to *Im*3*m*. The same authors reported that the space group of the Cub phase of ANBC-18 is *Ia*3*d* [9, 12]; it was therefore reasonably assumed at that time that the formation of different types of cubic phase between ANBC-*n* and ACBC-*n* series is probably due to the effect of the lateral substituent *X* (*X*=NO_2 or CN). Now that we know the type of cubic phase in the ANBC-*n* series as a function of *n* [26, 27], the earlier assumption has to be examined and it is of great interest to investigate the change of the Cub phase type with *n*. This paper reports the results of X-ray diffraction studies on ACBC-16.

2. Experimental

2.1. *Preparation*

ACBC-16 was synthesized at Technische Universität Darmstadt. The quality of the sample was checked by elemental analysis. Details are given in [34].

2.2. *Measurements*

The phase transitions were examined by differential scanning calorimetry (Seiko Denshi, DSC-210) with interface to a data station (Seiko Denshi, SSC 5000 system). The measurements were performed under a dry nitrogen flow of *c.* 40 ml min^{-1} and the scanning rate was 5 K min^{-1}. The texture of each mesophase was observed with a polarizing optical microscope (POM, Nikon Optiphot-pol XTP-11) equipped with a hot stage (Mettler FP-82) and a central processor (Mettler FP80) at a heating/cooling rate of 5 or 10 K min^{-1}.

X-ray diffraction (XRD) patterns at elevated temperatures were obtained for powder samples sandwiched with two 12.5 μm thick Kapton windows or filled in thin glass capillaries 1.5 mm in diameter; two set-ups were used.

In the first set-up (A), synchrotron radiation was used as the X-ray source at the Photon Factory (PF) of the high energy accelerator research organization (KEK), Tsukuba, Japan, where the small angle X-ray scattering equipment for solutions (SAXES) was installed on beamline BL-10C. The SAXES employs point-focusing optics with a double-flat monochromator followed by a bent cylindrical mirror. The incident beam intensity ($\lambda=0.1488$ nm) was monitored by an ionization chamber to correct for a minor decrease in intensity during the measurements. The scattered intensity was detected by a linear position-sensitive proportional counter (PSPC) with 512 channels. The geometry was further checked with chicken tendon collagen, which gives a set of sharp diffraction lines corresponding to a spacing of 65.3 nm. Details of the optics and instrumentation are described elsewhere [37]. The sandwiched sample was placed in a hot stage (Mettler FP82HT), and the temperature controlled within ± 0.1°C by a central processor (Mettler FP90). The accuracy of the temperature was checked using a calibrated iron–constantan thermocouple. The accumulation time for each measurement was 180 s.

In the second set-up (B), Rigaku NANO-Viewer IP system was used and operated with a copper target at 45 kV and 60 mA. The CuK_α radiation ($\lambda=0.154$ nm) was focused with a Confocal Max-Flux (CMF) mirror and collimated into the sample capillary using a three-slits system. The scattered X-rays were recorded on a two-dimensional imaging plate (IP, Fuji Film BAS-IP

SR 127) camera with an effective area of $11.5 \times 11.5\,cm^2$; the distance between the sample and the IP was about 67 cm. The geometry was further checked with chicken tendon collagen and by α-stearic acid. The latter sample gives a set of diffractions of 3.95 nm. The exposure time for each measurement was 600–1200 s, depending on the intensity obtained and the quality needed. The exposed IP film was read with an IP reader (Rigaku R-AXIS DS3C). The capillary sample, which was flame-sealed, was placed in a mid-temperature cell designed for this system, and the temperature was controlled within $\pm 0.1^{\circ}C$ by a Rigaku Themo Plus 2 system. The accuracy of the temperature was checked using a calibrated iron–constantan thermocouple.

3. Results

Figure 1 shows DSC curves of ACBC-16 taken at a scanning rate of $5\,K\,min^{-1}$. On heating, two liquid crystalline phases, a smectic C (SmC) and a cubic (Cub) phase, appear above the melting temperature (398 K).

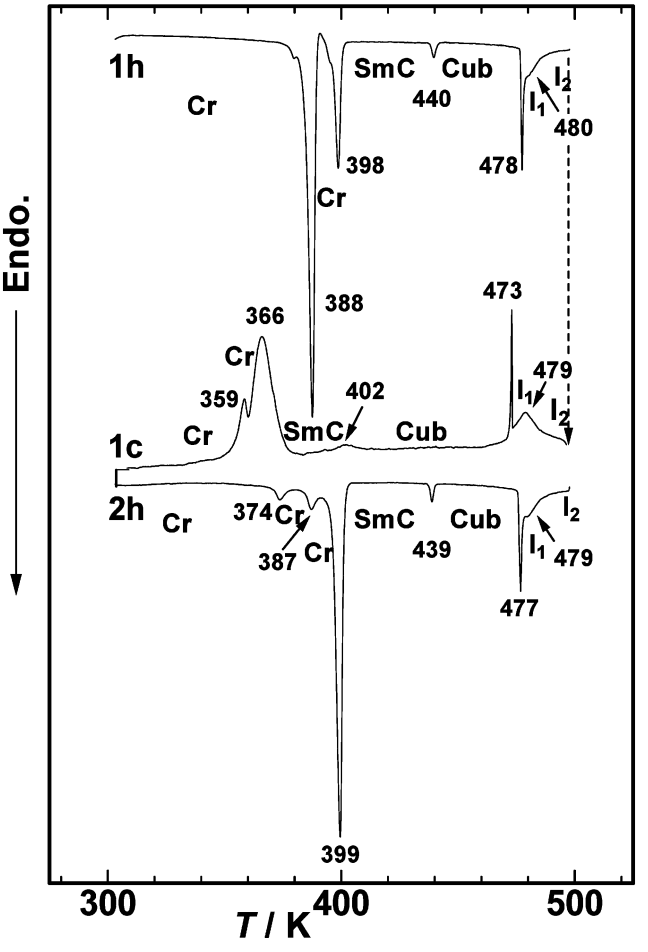

Figure 1. DSC thermogram of ACBC-16 recorded at a rate of $5\,K\,min^{-1}$.

The optical microscopic texture of the former phase was characterized by the appearance of a typical SmC schlieren texture under crossed polarizers, and the transition to the latter phase was easily identified by a slow growth of completely dark texture and thus optically isotropic areas with polygonal shapes. In the isotropic liquid (I) state, an endothermic shoulder peak is seen at 480 K on heating. This peak is reversible with temperature and a broad exothermic peak is seen at 479 K on cooling. In the DSC chart, we label the states below and above this event as I_1 and I_2 phases, respectively. This will be discussed later in more detail. Transition temperatures are essentially the same as in previous reports [3, 34].

When the corresponding nitro-substituted analogue ANBC-16 is cooled from the I phase, a mosaic texture is often observed before the formation of the Cub phase [2–4, 8, 32, 33, 38], which has been assigned to the columnar or tetragonal ($I4_1/acd$) phases. Although the existence of a similar texture was reported for ACBC-16 [3], we observed no such texture.

Figure 2 shows the XRD patterns of ACBC-16 taken at 433.8 K. The temperature is in the Cub region. The two-dimensional IP image shown in figure 2(*a*) is a spot-like pattern arising from a very small number of fairly large domains. The circular–averaged pattern is shown in figure 2(*b*). Five peaks are seen with the following ratios of reciprocal spacings: $\sqrt{3}$: $\sqrt{4}$: $\sqrt{7}$: $\sqrt{8}$: $\sqrt{10}$. Since the ratio $\sqrt{7}$ is not compatible with any cubic lattice, the sequence of numbers must be doubled and the obtained ratios are $\sqrt{6}$: $\sqrt{8}$: $\sqrt{14}$: $\sqrt{16}$: $\sqrt{20}$, corresponding to the Miller indices (2 1 1), (2 2 0), (3 2 1), (4 0 0), and (4 2 0). The diffractions from lower indices (1 0 0), (1 1 0), (1 1 1), (2 0 0), and (2 1 0) are all absent. Since ACBC-16 is achiral, the extinction rule observed matches the space group $Ia3d$ [$(h\,k\,l)$ with $h+k+l=2n$, $(0\,k\,l)$ with $k=2n$ and $l=2n$, $(h\,h\,l)$ with $2h+l=4n$, and $(0\,0\,l)$ with $l=4n$ are observable, where n=integer and h, k and l are permutable], which is the most frequently observed Cub phase type [14, 28]. Moreover, the following two features also support the above assignment: (i) only two peaks labelled (2 1 1) and (2 2 0) are notably seen, and (ii) the two-dimensional pattern is composed of several spots, reflecting the existence of large Cub domains being easily grown. The cell parameter at this temperature was $a=(11.26 \pm 0.02)$ nm.

Figure 3 shows the temperature variation of the circular-averaged XRD patterns. An important point to note is that in the Cub phase temperature region, both on heating and on cooling, all the observed patterns are essentially the same: two intense peaks of (2 1 1) and (2 2 0) reflections and a few faint peaks such as (3 2 1),

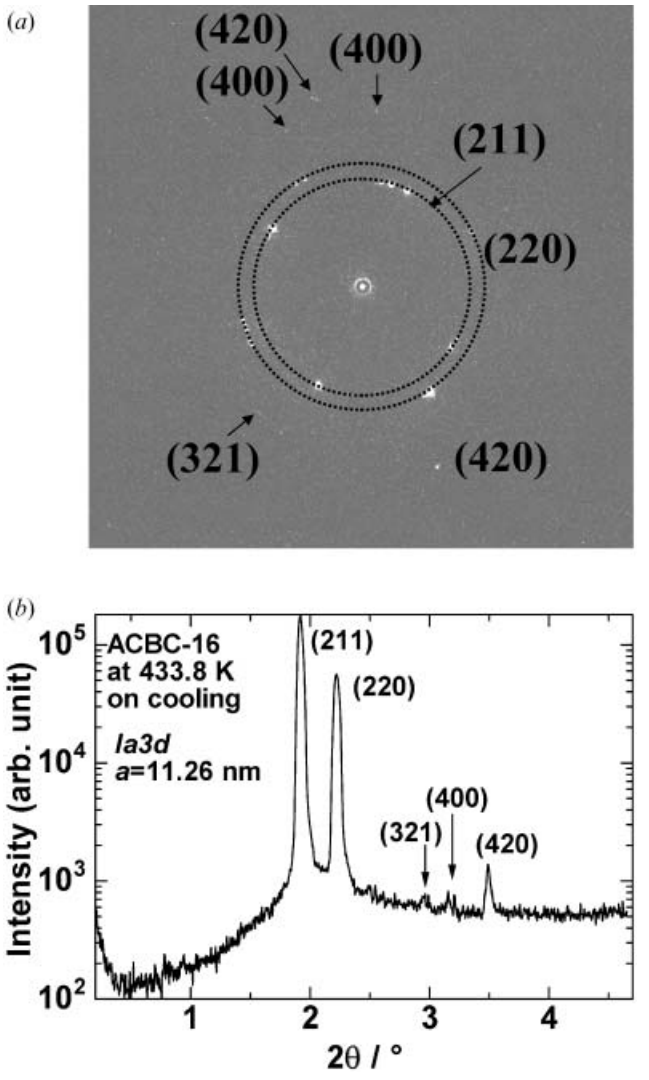

Figure 2. (*a*) 2D-XRD pattern and (*b*) circular-averaged pattern of ACBC-16 at 433.8 K on cooling.

(4 0 0), (4 2 0) and (3 3 2). This implies that the *Ia*3*d* type is formed in the whole temperature region of the Cub phase, both on heating and on cooling. Another important feature is a broad halo seen at around $2\theta=2^\circ$ in the I_1 and I_2 phase region, both on heating and on cooling. The halo itself suggests the presence of a short range ordering of the order of several nm.

To evaluate the correlation length ξ, the observed pattern was fitted using the following Ornstein–Zernike type function [22, 39, 40]:

$$I(q)=I_0+\left\{I(q^*)\Big/\left[1+\xi^2(q-q^*)^2\right]\right\}.$$

Here, the intensity is expressed as a function of scattering vector q; q is defined as $(4\pi/\lambda)\sin\theta$ with 2θ=scattering angle, I_0 is the constant background, and q^* is the q value at which the halo shows a maximum. The results are shown in figure 4. The ξ value is around 4 nm in the I_1 phase and 2 nm in the I_2 phase. The same evaluation was made for ANBC-16, and the obtained value was 4 nm in the I_1 phase (at 476.9 K) and 2 nm in the I_2 phase (at 485.3 K) [41], giving completely the same results as those for ACBC-16.

In our set-up B, the IP plate was not fixed in the NANO-Viewer optics during the experiments. It must be removed from the optics to read the pattern after being exposed to scattered X-rays. Thus, the IP recoding usually contains some uncertainty concerning the position of the direct X-ray beam. We determined the position of the direct beam using the fact that the diffracted spots are distributed in rings. Averaging the positions of the centres for these rings can give the position of the direct beam, in the case that the sample is composed of so many domains oriented isotropically. When the sample shows a Cub phase, however, the irradiated sample often consists of insufficient domains oriented isotropically, but consists of a small number of fairly large domains. In that case, this method contains a considerable experimental error in the position of the direct beam, and thus, in the cell parameters. To determine the temperature dependence of the cell parameter precisely, we used the set-up A described in §2.2.

Figure 5 shows the plots of *d*-spacing versus temperature (T) for ACBC-16. In the figure, open and filled symbols represent the data on heating and cooling, respectively. Three points are noted:

(1) The slope of the d versus T plot is always slightly negative. This indicates the contraction of the SmC layer thickness and the unit lattice with increasing T in the SmC phase and in the Cub region, respectively. These trends were also observed for all ANBC-*n* homologues [26, 27] and other Cub phase-forming materials [28, 38, 42]. The increment (α) of the cubic lattice constant (a) with T was calculated by using the relation $\alpha=(1/a)(\partial a/\partial T)$. The result is $\alpha=-3\times10^{-4}\,\mathrm{K}^{-1}$ on heating and $\alpha=-2\times10^{-4}\,\mathrm{K}^{-1}$ on cooling.

(2) The variation of the SmC layer spacing with T is approximately linear and smoothly connected to the temperature variation of Cub (2 1 1) spacing across the phase boundary. This suggests the existence of an epitaxial relationship between the two phases. This trend was also observed for the n=15–17 members of ANBC-*n* [26, 27] and very often seen for lyotropic cubic systems at the lamellar to *Ia*3*d*-Cub phase transition [43].

(3) Since in this case we used a one-dimensional PSPC counter as a detector for scattered X-rays, only one

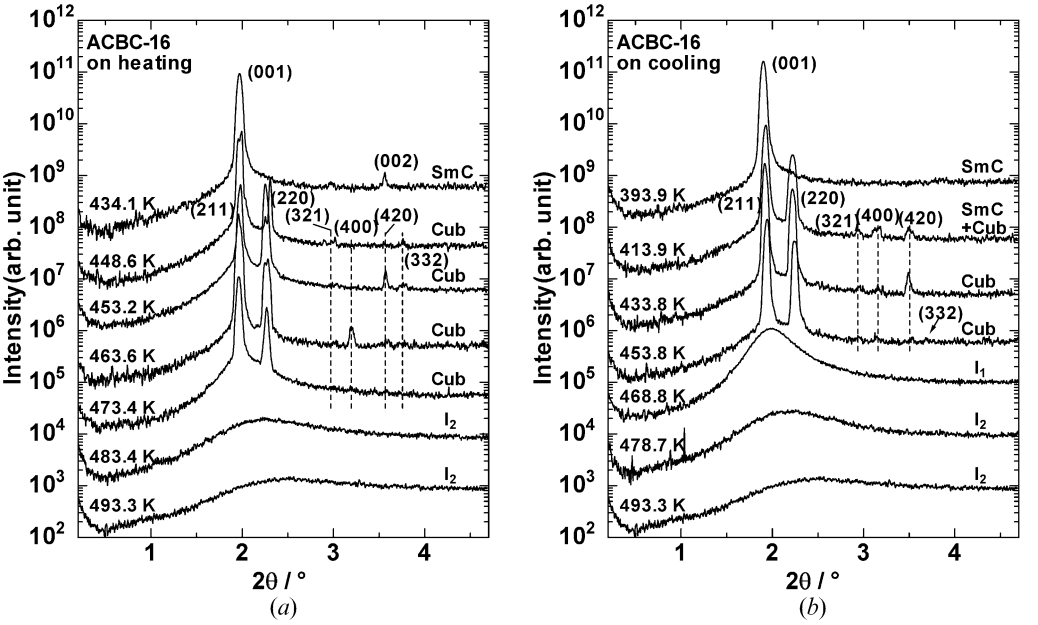

Figure 3. Circular-averaged XRD pattern of ACBC-16 as a function of temperature (*a*) on heating and (*b*) on cooling. The scale of the ordinate corresponds to the pattern recorded at 493.3 K, and other patterns are shifted by the factor of 10 for clarity. Miller indices are also shown for each pattern.

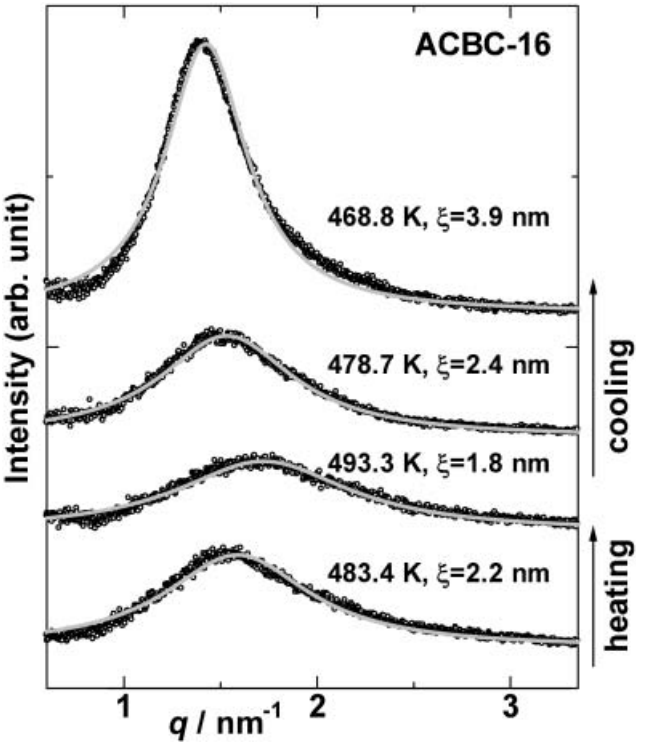

Figure 4. Circular-averaged XRD pattern (o) as a function of temperature in the vicinity of the Cub to I_1 transition temperature and above. The solid curves are the fit by the Ornstein–Zernike type function (see text), and the correlation length ξ as obtained from the fits are shown in the right side.

reflection peak was detected in the small angle region on cooling, most probably due to the spot-like pattern, as seen in figure 2 (*a*). The *d* versus *T* plot for this peak (filled circles) is completely superposed with the corresponding plot for the Cub (2 1 1) spacing on heating (open circles), except that the region itself extends over the lower temperature side owing to the supercooling effect. Thus, the peak detected on cooling is assigned also to the Cub (2 1 1) reflection, which confirms again that the type of the Cub phase for this compound is the same both on heating and on cooling.

Since the Cub phases of both ACBC-16 and ANBC-16 belong to the same symmetry *Ia*3*d*, the miscibility of the two Cub phases is worth investigating. Figure 6 presents the phase diagram for the binary system of ACBC-16 and ANBC-16. The boundaries of the regions in the diagram were determined by DSC with a cooling rate of $10\,\mathrm{K\,min^{-1}}$ from the I_2 phase, and further confirmed by POM. As expected, the two Cub phases are completely miscible. The smectic A (SmA) phase region vanishes when the molar fraction of ACBC-16 ($x_{\mathrm{ACBC\text{-}16}}$) is around 0.3. On the other hand, the Cub and SmC phases are divided by a wide biphasic region, resulting in a very narrow SmC region at about $x_{\mathrm{ACBC\text{-}16}} > 0.3$. The crystalline states of the mixture were complicated and are incompletely shown in the figure.

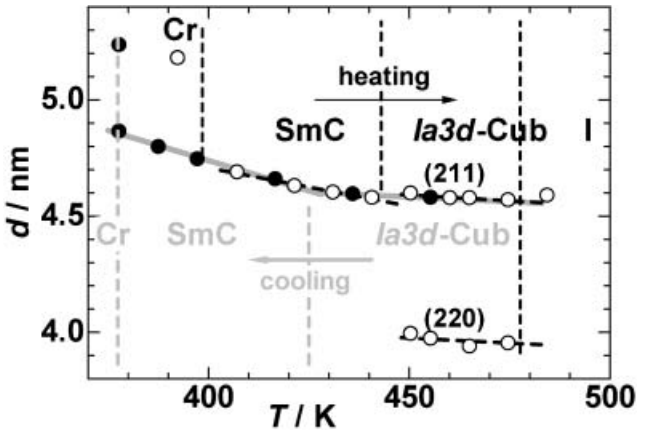

Figure 5. Plots of d-spacing versus temperature (T) for ACBC-16, where open and filled symbols represent the data on heating and cooling, respectively.

4. Discussion

4.1. *Comparison between the ACBC-n and ANBC-n series*

In figure 7, we compare the transition temperatures of ACBC-16 and -18 with the phase diagram of the ANBC-n series. The mesogens ANBC-n with $n \geqslant 15$ exhibit two Cub phases and in the shorter alkoxy chain homologues, a boundary of the *Ia*3*d*-Cub II and *Im*3*m*-Cub I phases exists between $n=18$ and 19 [26]. In the case of the ACBC-n series, on the other hand, the present work revealed that the type of the Cub phase of ACBC-16 is *Ia*3*d*, similarly to that of the corresponding nitro analogue ANBC-16; and previous work reported that the Cub phase of ACBC-18 is of *Im*3*m* type [9, 12],

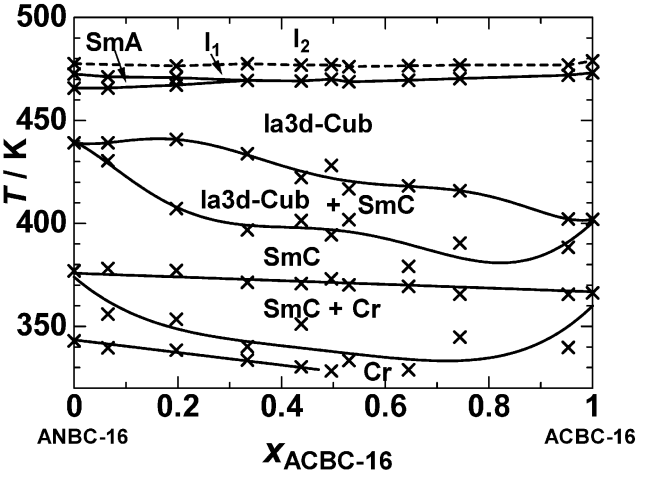

Figure 6. Phase diagram for the binary mixture of ACBC-16 and ANBC-16, where $x_{\mathrm{ACBC\text{-}16}}$ is the molar fraction of ACBC-16 in the mixture. The diagram was determined by DSC with a cooling rate of 10 K min^{-1} from the I_2 phase.

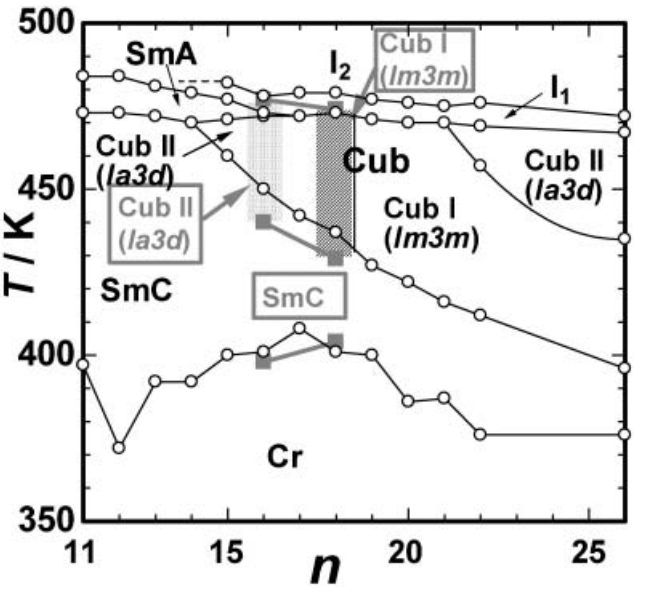

Figure 7. Phase diagram of ANBC-n (o) and ACBC-n (■), where n is the number of carbon atoms in the alkoxy group: Cr=crystal; SmC/A=smectic C/A; Cub=cubic; I_1, I_2=isotropic liquid phases; the phase types for ACBC-n are in squares. Transition temperatures for ACBC-16 are based on the DSC data of this work, and those for ACBC-18 are cited from [3]; identification of the phase type for ACBC-18 is after [9, 12]. Transition temperatures and identification of the phase type for ANBC-n are cited from [10, 26].

which is formed for the longer alkoxy chain homologues with $n \geqslant 19$ in the ANBC-n series. Hence, it is considered that the dependence of the Cub phase type on the alkoxy chain length n in the ACBC-n series is essentially the same as that in the ANBC-n series, but shifted towards shorter n by 1 or 2. Therefore, the earlier assumption that the different type of Cub phases formed between ANBC-18 and ACBC-18 may be due to the effect of the lateral substituent X (X=NO_2 or CN) [12] seems to be unreasonable.

It is also of interest to compare the Cub cell parameter a of ACBC-16 with those of the ANBC-n series. The cell parameters at temperatures near 450 K for ANBC-n are summarized in [27]. The a value of ACBC-16 at 453.2 K was $a=(11.03 \pm 0.04)$ nm, which is 2.5% larger than the value of ANBC-16 (10.76 nm at 459.2 K) and close to the value of ANBC-17 (10.94 nm at 453.3 K) or ANBC-18 (11.39 nm at 450.5 K). Moreover, if we regard ACBC-16 as 'ANBC-17.5', the binary phase diagram shown in figure 6 would correspond to the phase diagram of the ANBC-n series between $n=16$ and 17.5 in figure 7. Thus, the $x_{\mathrm{ACBC\text{-}16}}$ value at which the SmA phase region vanishes in figure 6 might correspond to $n=16.5$, approximately in agreement with the n dependence of the SmA phase region in the ANBC-n diagram. On the other hand,

temperature-dependent layer spacings of the SmC phase (L_{SmC}) of ACBC-16, ANBC-17 [26], and ANBC-18 [26] may be expressed as follows:

for ACBC-16, $L_{SmC}/nm = 4.64 - (3.29 \times 10^{-3})(T/K - 420)$ (399 K $\leqslant T \leqslant$ 443 K);
for ANBC-17, $L_{SmC}/nm = 4.54 - (1.67 \times 10^{-3})(T/K - 420)$ (407 K $\leqslant T \leqslant$ 442 K);
for ANBC-18, $L_{SmC}/nm = 4.74 - (3.76 \times 10^{-3})(T/K - 420)$ (400 K $\leqslant T \leqslant$ 437 K).

Comparison of these values shows that the layer spacing in ACBC-16 is between those of ANBC-17 and -18. This result also supports the above trend that the effective molecular length of ACBC-16 corresponds to a mid value between the two molecular lengths of ANBC-17 and -18. Therefore, the replacement of the NO_2 group with the CN group causes an apparent extension effect of the alkoxy chain length compared with ANBC-16. However, a question arises as to the molecular origin of this observation.

Probably, three factors are to be considered, electronic effect, steric effect, and alkyl chain versus aromatic core repulsion. First, we compare the electronic effects of NO_2 and CN groups. The tabulated values of the dipole moments are 4.22 D (1 D = 3.33×10^{-30} C m) for NO_2 and 4.18 D for CN [44]. Thus, the dipole moments of both groups are almost the same, which cannot therefore be the main origin for the apparent extension effect in ACBC-16.

Second, we consider the difference in the steric effect arising from each group. Molecular models of the dimeric structures of ACBC-16 and ANBC-16 were optimized on the basis of the AM1 force-field method using CS Chem3D Pro™ (produced by Cambridge Soft Corporation, Inc.). The optimized molecular models are shown in figure 8. As expected, the shapes and lengths of the molecular models of both compounds are almost identical. For both compounds, the estimated lengths of the alkoxy chains in the extended form are 2.07 nm†, and the distances between two ether oxygen atoms, which corresponds to the length of the aromatic core part in each dimeric form, are 2.42 nm. The lateral extensions of both compounds were estimated as the maximum distance from the centre line connecting the 4- and 4′- positions of the biphenyl core to the van der Waals surface of the oxygen atom (with a radius r of 0.14 nm) in the NO_2 group or of the nitrogen atom (r = 0.15 nm) in the CN group. The estimated distances in both cases are unexpectedly the same and 0.49 nm, which results in the same length-to-breadth ratio for both compounds. However, as expected from the fact that the NO_2 group is composed of three atoms whereas the CN group is of two atoms, both groups have different volumes. According to Bondi [46], the van der Waals volume of the NO_2 group is 0.0279 nm^3 and that of the CN group is 0.0244 nm^3; the former is 14% larger than the latter. This difference would probably cause a slightly different lateral packing. That is, the more bulky NO_2 group would cause a slightly larger slippage along the molecular long axis, which corresponds to a slightly larger tilt in the SmC layer, which would also lead to a slightly smaller Cub cell parameter for ANBC-16 than for ACBC-16. Therefore, the two lateral substituents provide the same molecular breadth but bring about different steric effects on the lateral packing.

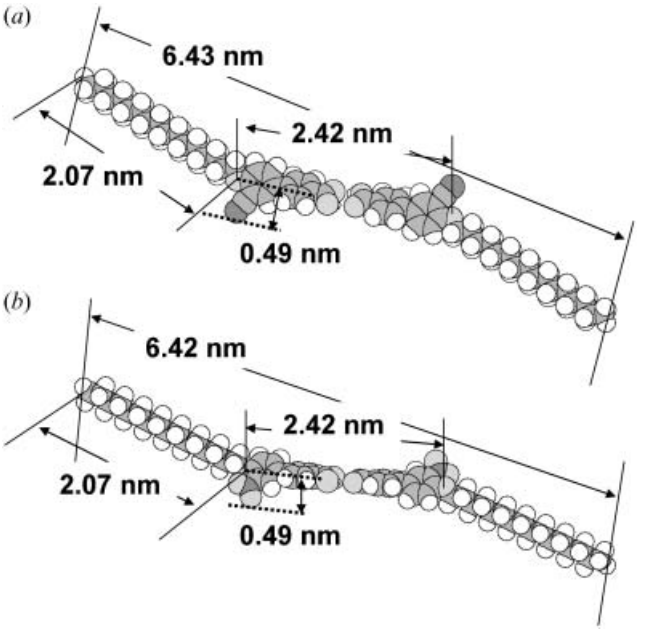

Figure 8. Optimized molecular models of (*a*) ACBC-16 and (*b*) ANBC-16 dimer.

By analogy with microphase-separation in block copolymer systems, Yoneya *et al.* estimated the incompatibility parameter between the two parts ($\chi_{core\text{-}chain}$) and the volume fraction of the core part (f_{core}) for several low molecular mass liquid crystalline systems. Although their calculations do not rigorously include the temperature effect, a good correspondence was found between the two systems [47]. This encourages us to compare the volume fractions of the

†As in similar calculations, the estimation corresponds to that at T = 0 K. At finite temperatures where the alkoxy chains obtain complete flexibility, the chain length becomes as short as about 70% of the extended form on the basis of Flory's theory [45]. However, this temperature effect would be the same on both compounds, producing no meaningful difference.

alkyl part of ANBC-16 and ACBC-16. We first calculated the mass ratio of the alkyl chain to the total molecular mass. The molecular masses of $C_{16}H_{33}$, $C_{17}H_{35}$, and $C_{18}H_{39}$ chains are 225.44, 239.46 and 253.49, respectively, and those of the $OC_6H_3XC_6H_4COOH$ part are 258.21 for $X=NO_2$ and 238.22 for $X=CN$. For ANBC-*n*, the mass ratios of the alkyl chain to the total are, respectively, 0.466, 0.481 and 0.495 for $n=16$, 17, and 18; whereas the corresponding value for ACBC-16 is 0.486, which just lies between the values of ANBC-17 and -18. The core parts of both compounds are the same except for their lateral substituent X. Assuming that for simplicity the density of both the alkyl tail and core parts are the same, the mass ratio of each part corresponds to the volume ratio. Thus, the third factor, alkyl chain versus aromatic core repulsion, can also explain the apparent extension effect of the alkyl chain length by the CN group compared with ANBC-16. However, the quasi-binary approximation seems too simplified for this problem.

At this stage, we can only say that the second or the third factor, or the combination of these two is most probable for the main molecular origin. Since CN and NO_2 groups have different shapes, it is at least reasonable that the interactions between neighbouring CN or NO_2 groups would cause slightly different stacking of the molecules both in the SmC and Cub phases between ACBC-16 and ANBC-16.

4.2. *DSC 'hump' in the isotropic liquid state*

In a previous paper [34], Sorai and co-workers found that an ACBC-16 sample supercooled from the I state to just below the Cub–I_1 phase transition exhibits a broad endothermic peak on subsequent heating. This and the reversibility of the peak shown in figure 1 suggest that the broad peak seen in the I state often called the DSC 'hump' is not necessarily associated with the formation of the Cub phase. A similar kind of broad peak was observed for a homologous series of ANBC-*n* regardless of whether Cub phases were seen [8, 10, 16, 22], and also observed for the binary system ANBC-8/*n*-tetradecane with a high content of the paraffinic carbon atoms, although the system exhibits no Cub phases [13]. These observations also support the suggestion that this peak is not associated with the Cub phase formation. Furthermore, many other examples have been reported that the melting processes of twist grain boundary (TGB) phases [48] and blue phases (BP) [49], and phase transitions from SmA to the isotropic [50], disorganized liquid appear with first a sharp peak followed by a broad hump. Goodby *et al*. [48] suggested the possibility of the assignment of the hump to the destruction of shorter range order than that of the original length. In the case of the melting of Cub, BP and TGB phases, the inter-aggregate, long range order characterized by the lattice dimension or the distance between two neighbouring dislocation lines is lost at the first sharp peak temperature, called 'lattice melting', but there still remain the constituent aggregates, which would be gradually destroyed with the broad hump in the higher temperature region. In the case of the SmA phase, the long range, layer stacking order along the layer normal would be lost at the first sharp peak. It can be said that the existence of two different distance scale orders, the inter-aggregate, long range order and the intermolecular, shorter range order within the aggregates, is common for all these examples; in the latter ordering, the presence of attractive forces such as lateral dipole–dipole interaction is important for binding molecules into an aggregate (rod-like micelle in Cub and BP, smectic layers slab in TGB, and smectic layer in SmA phases).

Returning to the ANBC-*n* systems, it is strongly suggested that the broad peak on heating is also related to the dissociation of carboxylic dimers, on the basis of the infrared spectral results [10, 11, 19] and the comparison between the observed enthalpy change and the dissociation enthalpy involved [15]. Therefore, the destruction of the short range correlation between the remnant aggregates is seen as a cooperative phenomenon coupled with the dissociation of carboxylic dimers [15, 22]. This cooperative nature, i.e. the dissociation of carboxylic dimers as a driving force for the destruction of the short range correlation, can explain the appearance of the broad hump commonly observed around 470 K irrespective of the appearance of Cub phases in the ANBC-*n* and ACBC-*n* series.

The present work on ACBC-16 showed that the correlation length ξ in the I_1 phase is $\sim$4 nm, and the ξ value in the I_2 phase is $\sim$2 nm. On the other hand, in the *Ia*3*d*-Cub phase, the diameter and length of constituent rod-like micelles are approximately expressed as $D=(a\sqrt{5})/4$ and $L=a/\sqrt{8}$, respectively [21, 22]. The estimated D and L values were 6.1 and 3.9 nm, respectively, which is close to the ξ value in the I_1 phase. This suggests that remnants of the Cub phase exist in the I_1 phase. The close resemblance of the D and L values to the ξ value in the I_1 phase was also reported for a very long alkoxy chain compound ANBC-26 [22]. As already mentioned, an important point is that the I_1 phase is not a transient state but a thermodynamic equilibrium phase. Therefore, it is more reasonable to imagine that the I_1 phase acts as a mesh (or sponge) phase seen for lyotropic systems [51–53]. The same assignment was made by Sorai *et al*. for the intermediate temperature region divided by a sharp Cub to

lamellar L_α phase transition peak and a subsequent broad hump in some surfactant–water systems [54, 55] (these authors referred to the intermediate region as a perforation fluctuation layer (PFL) phase).

In the I_2 phase, the observed ξ is $\sim$2 nm, which is close to the alkyl chain length or the aromaitc core size of ACBC-16 (see figure 8), suggesting the presence of spherical micelles composed of several molecules of which some are hydrogen–bonded and some are not. Since the correlation length corresponds to the segregation of the two incompatible parts of the single molecule, the origin of the peak is quite similar to the mechanism for the correlation hole in block copolymer systems [40, 56]. The observed peak diminishes with increasing temperature, and thus the micelles are in a transient state.

Acknowledgements

We first thank Dr Yuji Naruse and Prof. Keiichi Moriya at Gifu University and Prof. Kazuchika Ohta at Shinshu University for stimulating discussions. We also thank Ms Shouko Nishiura and Mr Hiroyuki Mori at Gifu University and Ms Mayumi Ikeda at Osaka University for their experimental help. This work was supported by Grant-in-Aid for Scientific Research on Priority Areas (A), 'Dynamic Control of Strongly Correlated Soft Materials' (No. 413/14045232) from the Ministry of Education, Science, Sports, Culture, and Technology, Japan, and by Grant-in-Aid for Scientific Research (C) 14550846 from the Japan Society for the Promotion of Science (JSPS), both of which were given to S.K., and by Grant-in-Aid for Scientific Research (B) 15350110 from JSPS, given to K.S. Beam time at PF-KEK provided by Program 2002G095 is also acknowledged.

References

[1] G.W. Gray, B. Jones, F. Marson. *J. Chem. Soc.*, 393 (1957).
[2] G.W. Gray, J.W. Goodby, *Smectic Liquid Crystals*, pp. 68–81, Leonard Hill, Glasgow (1984): including earlier references on thermotropic cubic phases.
[3] G.W. Gray. *Zehn Arbeiten über Flüssige Kristalle* Kongress- und Tagungsberichte der Martin Luther-Universität, Halle-Wittenberg, pp. 22–42 (1986).
[4] D. Demus, G. Kunicke, J. Neelsen, H. Sackmann. *Z. Naturforsch.*, **23a**, 84 (1968).
[5] G. Pelzl, H. Sackmann. *Symp. Chem. Soc., Faraday Div.*, **5**, 68 (1971).
[6] S. Diele, P. Brand, H. Sackmann. *Mol. Cryst. Liq. Cryst.*, **17**, 163 (1972).
[7] A. Tardieu, J. Billard. *J. Phys. (Paris) Coll.*, **37**, C3-79 (1976).
[8] D. Demus, D. Marzotko, N.K. Sharma, A. Wiegeleben. *Krist. Technol.*, **15**, 331 (1980).
[9] A.-M. Levelut, Y. Fang. *Coll. Phys., Coll.*, **51**, C7-229 (1990).
[10] S. Kutsumizu, M. Yamada, S. Yano. *Liq. Cryst.*, **16**, 1109 (1994).
[11] S. Kutsumizu, R. Kato, M. Yamada, S. Yano. *J. Phys. Chem., B*, **101**, 10666 (1997).
[12] A.-M. Levelut, M. Clerc. *Liq. Cryst.*, **24**, 105 (1998).
[13] K. Saito, A. Sato, M. Sorai. *Liq. Cryst.*, **25**, 525 (1998).
[14] S. Diele, P. Göring. *Handbook of Liquid Crystals*, D. Demus, J. Goodby, G.W. Gray, H.-W. Spiess, V. Vill (Eds), pp. 887–900, Wiley-VCH, Weinheim (1998): this is the most comprehensive review on the thermotropic cubic phases and a complete documents list until 1998 is given.
[15] A. Sato, K. Saito, M. Sorai. *Liq. Cryst.*, **26**, 341 (1999).
[16] S. Kutsumizu, T. Yamaguchi, R. Kato, S. Yano. *Liq. Cryst.*, **26**, 567 (1999).
[17] A. Sato, Y. Yamamura, K. Saito, M. Sorai. *Liq. Cryst.*, **26**, 1185 (1999).
[18] S. Kutsumizu, T. Ichikawa, S. Nojima, S. Yano. *Chem. Commun.*, 1181 (1999).
[19] S. Kutsumizu, T. Yamaguchi, R. Kato, T. Ichikawa, S. Yano. *Mol. Cryst. Liq. Cryst.*, **330**, 359 (1999).
[20] D.S. Shankar Rao, S.K. Prasad, V. Prasad, S. Kumar. *Phys. Rev. E.*, **59**, 5572 (1999).
[21] S. Kutsumizu, H. Kobayashi, N. Nakamura, T. Ichikawa, S. Yano, S. Nojima. *Mol. Cryst. Liq. Cryst.*, **347**, 239 (2000).
[22] S. Kutsumizu, T. Ichikawa, M. Yamada, S. Nojima, S. Yano. *J. Phys. Chem. B*, **44**, 10196 (2000).
[23] K. Saito, T. Shinhara, M. Sorai. *Liq. Cryst.*, **27**, 1555 (2000).
[24] Y. Maeda, G.-P. Cheng, S. Kutsumizu, S. Yano. *Liq. Cryst.*, **28**, 1785 (2001).
[25] K. Saito, T. Shinhara, T. Nakamoto, S. Kutsumizu, S. Yano, M. Sorai. *Phys. Rev. E*, **65**, 031719 (2002).
[26] S. Kutsumizu, K. Morita, T. Ichikawa, S. Yano, S. Nojima, T. Yamaguchi. *Liq. Cryst.*, **29**, 1447 (2002).
[27] S. Kutsumizu, K. Morita, S. Yano, S. Nojima. *Liq. Cryst.*, **29**, 1459 (2002).
[28] S. Diele. *Curr. Opin. Colloid Interface Sci.*, **7**, 333 (2002).
[29] S. Kutsumizu. *Curr. Opin. solid State Mater. Sci.*, **6**, 537 (2002).
[30] K. Saito, M. Sorai. *Chem. Phys. Lett.*, **366**, 56 (2002).
[31] M. Sorai, K. Saito. *Chem. Rec.*, **3**, 29 (2003).
[32] Y. Maeda, S.K. Prasad, S. Kutsumizu, S. Yano. *Liq. Cryst.*, **30**, 7 (2003).
[33] Y. Maeda, K. Morita, S. Kutsumizu. *Liq. Cryst.*, **30**, 157 (2003).
[34] M. Sorai, K. Saito, T. Nakamoto, M. Ikeda, Y.G. Galyametdinov, I. Galyametdinova, R. Eidenschink, W. Haase. *Liq. Cryst.*, **30**, 861 (2003).
[35] G. Etherington, A.J. Leadbetter, X.J. Wang, G.W. Gray, A. Tajbakhsh. *Liq. Cryst.*, **1**, 209 (1986).
[36] G. Etherington, A.J. Langley, A.J. Leadbetter, X.J. Wang. *Liq. Cryst.*, **3**, 155 (1988).
[37] T. Ueki, Y. Hiragi, M. Kataoka, Y. Inoko, Y. Amemiya, Y. Izumi, H. Tagawa, Y. Muroga. *Biophys. Chem.*, **23**, 115 (1985).
[38] A.-E. Levelut, B. Donnio, D. Bruce. *Liq. Cryst.*, **22**, 753 (1997).
[39] L.A. Feigin, D.I. Svergun. *Structure Analysis by Small-Angle X-ray and Neutron Scattering*, p. 243, Plenum, New York (1987).

[40] M.O. de la Cruz, I.C. Sanchez. *Macromolecules*, **19**, 2501 (1986).
[41] S. Kutsumizu, unpublished results.
[42] V. Percec, W.-D. Cho, G. Ungar, D.J.P. Yeardley. *J. Am. Chem. Soc.*, **123**, 1302 (2001).
[43] Y. Rançon, J. Charvolin. *J. Phys. Chem.*, **92**, 2646 (1988).
[44] D.R. Lide (Ed.), *CRC Handbook of Chemistry and Physics* 76th Ed., pp. 9–50, CRC Press, Boca Raton (1995).
[45] P.J. Flory. *Statistics of Chain Molecules* Chapter V, Wiley, New York (1969).
[46] A. Bondi. *J. Phys. Chem.*, **68**, 441 (1964).
[47] M. Yoneya, K. Araya, E. Nishikawa, H. Yokoyama. *J. Phys. Chem. B*, **108**, 8099 (2004).
[48] J.W. Goodby, D.A. Dunmur, P.J. Collings. *Liq. Cryst.*, **19**, 703 (1995).
[49] Z. Kutnyak, C.W. Garland, J.L. Passmore, P.J. Collings. *Phys. Rev. Lett.*, **74**, 4859 (1995).
[50] E. Nishikawa, J. Yamamoto, H. Yokoyama. *J. Mater. Chem.*, **13**, 1887 (2003).
[51] B. Balinov, U. Olsson, O. Söderman. *J. Phys. Chem.*, **95**, 5931 (1991).
[52] M. Magalhães, D. Pusiol, M.E. Ramia, A.M.F. Neto. *J. Chem. Phys.*, **108**, 3835 (1998).
[53] C. Tschierske. *Curr. Opin. Colloid Interface Sci.*, **7**, 69 (2002).
[54] M. Nishizawa, K. Saito, M. Sorai. *J. Phys. Chem. B*, **105**, 2987 (2001).
[55] K. Saito, N. Kitamura, M. Sorai. *J. Phys. Chem. B*, **107**, 7854 (2003).
[56] P.-G. de Gennes. *Scaling Concepts in Polymer Physics*, pp. 62–68, Cornell University, Ithaca (1979).